

See discussions, stats, and author profiles for this publication at: <https://www.researchgate.net/publication/38076682>

# Soot Structure and Reactivity Analysis by Raman Microspectroscopy, Temperature-Programmed Oxidation, and High-Resolution Transmission Electron Microscopy

ARTICLE *in* THE JOURNAL OF PHYSICAL CHEMISTRY A · NOVEMBER 2009

Impact Factor: 2.69 · DOI: 10.1021/jp905639d · Source: PubMed

---

CITATIONS

61

READS

146

## 6 AUTHORS, INCLUDING:



Dangsheng Su

Chinese Academy of Sciences

643 PUBLICATIONS 13,139 CITATIONS

[SEE PROFILE](#)



Reinhard Niessner

Technische Universität München

593 PUBLICATIONS 12,227 CITATIONS

[SEE PROFILE](#)

# Soot Structure and Reactivity Analysis by Raman Microspectroscopy, Temperature-Programmed Oxidation, and High-Resolution Transmission Electron Microscopy

Markus Knauer,<sup>†</sup> Manfred E. Schuster,<sup>‡</sup> Dangsheng Su,<sup>\*,‡</sup> Robert Schlögl,<sup>‡</sup> Reinhard Niessner,<sup>†</sup> and Natalia P. Ivleva<sup>\*,†</sup>

Technische Universität München, Institute of Hydrochemistry, Chair for Analytical Chemistry, Marchioninistr. 17, D-81377 Munich, Germany, and Fritz-Haber-Institut der Max-Planck-Gesellschaft, Department of Inorganic Chemistry, Faradayweg 4-6, D-14195 Berlin, Germany

Received: June 16, 2009; Revised Manuscript Received: September 29, 2009

Raman microspectroscopy (RM), temperature-programmed oxidation (TPO), high-resolution transmission electron microscopy (HRTEM), and electron energy loss spectroscopy (EELS) were combined to get comprehensive information on the relationship between structure and reactivity of soot in samples of spark discharge (GfG), heavy duty engine diesel (EURO VI and IV) soot, and graphite powder upon oxidation by oxygen at increasing temperatures. GfG soot and graphite powder represent the higher and lower reactivity limits. Raman microspectroscopic analysis was conducted by determination of spectral parameters using a five band fitting procedure (G, D1–D4) as well as by evaluation of the dispersive character of the D mode. The analysis of spectral parameters shows a higher degree of disorder and a higher amount of molecular carbon for untreated GfG soot samples than for samples of untreated EURO VI and EURO IV soot. The structural analysis based on the dispersive character of the D mode revealed substantial differences in ordering descending from graphite powder, EURO IV, VI to GfG soot. HRTEM images and EELS analysis of EURO IV and VI samples indicated a different morphology and a higher structural order as compared to GfG soot in full agreement with the Raman analysis. These findings are also confirmed by the reactivity of soot during oxidation (TPO), where GfG soot was found to be the most reactive and EURO IV and VI soot samples exhibited a moderate reactivity.

## Introduction

Atmospheric aerosol particles form a class of air pollutants of great concern to air quality.<sup>1</sup> They are of central importance for atmospheric chemistry and physics, climate, and public health. Especially in urban area, soot particles emitted by diesel engines account for a major fraction of air pollutants. Present and future emission limits require that soot particles must be efficiently removed from diesel engine exhaust.<sup>2</sup> A wide range of particle trapping systems and exhaust aftertreatment technologies have been proposed and are currently under development. Continuously regenerating traps (CRT) or diesel particulate filters (DPF) which have been applied for this purpose have to be regenerated periodically by oxidation and gasification of the deposited soot.<sup>3–7</sup> The behavior of this regeneration step is strongly influenced by the structure and reactivity of the deposited soot particles.<sup>6,8–10</sup> Especially the formation of highly reactive soot would make it possible to perform this regeneration step at relatively low temperatures.<sup>10</sup>

The reactivity of soot is usually determined by temperature-programmed oxidation (TPO) experiments. The emitted carbon oxides are quantified by infrared (IR) spectroscopy<sup>4</sup> or mass spectrometry<sup>8</sup> and thereby the reactivity can be calculated by the amount of oxidized soot. For investigation of soot structure

high-resolution transmission electron microscopy (HRTEM) is usually applied. Recent measurements have shown that differences in the oxidation behavior of soot are associated with different microstructures.<sup>6,8,9</sup> However, TPO and HRTEM measurements are too demanding for routine analysis. Therefore it is highly desired to establish a rapid analytical tool indicating the reactivity of soot.

Raman spectroscopy can be applied to get detailed information about the reactivity of soot by determining the structure. This technique in general provides fingerprint spectra and allows a characterization of a wide range of chemical substances.<sup>11–13</sup> A correlation between the structure of soot and Raman spectroscopic parameters has already been discussed in literature.<sup>13–25</sup> It will be shown by morphological analysis that, in contrast to graphite samples, soot samples are characterized by a complex heterogeneous structure which includes graphitic and nonplanar molecular parts (basic structural units, BSUs) for which the Raman selection rules of graphite do not apply. Therefore, the convolution of both parts to a system of “disordered graphite” has to be taken into account when interpreting the D mode in Raman spectra of soot.

Raman microspectroscopy (RM), combining the analytical capabilities of Raman spectroscopy with the spatial resolution of an optical microscope, has already been applied for the characterization of soot structure and thereby reactivity. In a recent study, the experiments were performed in air (ca. 21% oxygen) as oxidant.<sup>24</sup> On the other hand we have demonstrated the potential of RM for the analysis of changes in the chemical structure of soot under conditions relevant for common diesel

\* Authors to whom correspondence should be addressed: e-mail natalia.ivleva@ch.tum.de, tel +49 89 2180 78238, fax +49 89 2180 78255; e-mail dangsheng@fhi-berlin.mpg.de, tel +49 30 8413 4464, fax +49 30 8413 4401.

<sup>†</sup> Technische Universität München.

<sup>‡</sup> Fritz-Haber-Institut der Max-Planck-Gesellschaft.

aftertreatment systems, i.e., oxidation at 5% oxygen in nitrogen<sup>26</sup> or nitrogen dioxide.<sup>19</sup>

In this study we combined RM and TPO to investigate changes in structure and reactivity of soot during oxidation by oxygen at increasing temperatures. For validation and better understanding of structural information obtained with RM, HRTEM and electron energy loss spectroscopy (EELS) were applied. EELS provides information about the electronical and chemical composition of the sample. By analyzing the ionization edge of carbon, it was possible to determine locally the bonding state of carbon atoms. We studied the correlation between Raman spectroscopic parameters, structural changes, and reactivity of GfG soot (spark discharge generated), EURO VI and IV diesel soot, and graphite powder, in a temperature range between 293 and 873 K with 5% oxygen in nitrogen, and obtained the relationship between structure and reactivity of soot particles from diesel exhaust.

## Experimental Section

**Materials.** To perform the experiments, different types of soot and carbonaceous material have been used. As reference for reactivity studies, we used GfG soot, generated by a spark discharge aerosol generator (GfG 1000, Palas, Germany) as upper reactivity limit, and a commercially available graphite powder or graphite ( $C \geq 99.0\%$ , particle size 1–2  $\mu\text{m}$ , Fluka/Sigma-Aldrich, Germany) as the lower reactivity limit. EURO IV soot samples were collected under world harmonized transient cycle (WHTC) conditions from the undiluted raw exhaust of a heavy-duty test engine that fulfills EURO 4 exhaust limits. Samples of EURO VI soot were taken under European transient cycle (ETC) conditions from the undiluted raw exhaust of a heavy-duty test engine that is designed to fulfill EURO 6 exhaust limits. All soot samples were deposited on Bekipor Fecralloy metal fiber filter material (Bekaert, Belgium) with a fiber diameter of  $\sim 10 \mu\text{m}$  and a filter diameter of 47 mm. For reference we used a highly oriented pyrolytic graphite (HOPG ZYB) from Mateck (Germany).

**Temperature-Programmed Oxidation.** A diesel exhaust aftertreatment model system<sup>4</sup> has been used to perform the oxidation experiments in a temperature range from 298 K up to 873 K with a total gas flow of 3 L/min of nitrogen including 5% of oxygen. The heating rate during the experiments was set to 5 K/min. The temperature of the filter substrate was adjusted with a temperature controller directly on the surface of the filter material, using a type K thermocouple. Analysis of oxidation products was done by FTIR spectroscopy using a IFS 66/s FTIR spectrometer (Bruker, Germany), equipped by a 2 L gas flow cell with an optical path length of 6.4 m.<sup>4</sup>

**Raman Microspectroscopy.** The Raman spectra have been recorded by a Renishaw 2000 Raman microscope system (Renishaw, U.K.), using laser wavelengths of  $\lambda_0 = 514 \text{ nm}$  (Ar<sup>+</sup> laser), 25 mW, and  $\lambda_0 = 633 \text{ nm}$  (He–Ne laser), 25 mW. Wavelength calibrations were performed with a silicon wafer by utilizing the first-order phonon band of Si at 520  $\text{cm}^{-1}$ . Spectra of the soot samples were taken before and after the oxidation process in the range of 800–2000  $\text{cm}^{-1}$  (Stokes shift) with a 50 $\times$  magnification objective and 10 s integration time. A defocused laser beam (diameter  $\approx 40 \mu\text{m}$ ) and 25% of the source power were applied to avoid laser-induced decomposition of the soot samples. The spectra were processed via WiRE 1.2 software (Renishaw, U.K.) running under GRAMS/32 (Thermo Galactic, USA).

After a multipoint baseline correction, spectra were fitted<sup>13,18,19</sup> by combination of four Lorentzian-shaped, G, D1, D2, and D4,

bands at about 1580, 1350, 1620, and 1200  $\text{cm}^{-1}$ , respectively, and one Gaussian-shaped D3 band at about 1500  $\text{cm}^{-1}$ . The G band was attributed to ideal and D1, D2, D4 to disordered graphitic lattice and nongraphitic BSU vibrations, respectively. The D3 band was only associated with the nongraphitic/molecular carbon content of soot. Mean values and standard deviations of the spectral parameters presented and discussed below were obtained from seven spectra recorded at different regions on the sample.

**High-Resolution Transmission Electron Microscopy.** A Philips TEM/STEM CM 200 FEG transmission electron microscope (Philips, Netherlands) equipped with a field-emission gun was used to study the morphology and microstructure of untreated and partially oxidized soot particles. The acceleration voltage was set to 200 kV. A point resolution of 2.1 Å and a spatial resolution of 1.4 Å are obtainable with this technique. To avoid any faults in interpreting the image contrast, images of the soot particles were taken without underlying carbon film. The soot particles were ultrasonically dispersed in chloroform, and then a drop of the solution was deposited on a holey C/Cu TEM grid to be used for TEM and HRTEM characterization. For particle size and curvature analysis of soot samples at least 15 HRTEM images were taken into account.

**Electron Energy Loss Spectroscopy.** Electron energy loss spectra were recorded with a Gatan Image Filter (GIF Tridiem; Gatan, USA) mounted below the Philips CM 200 FEG. The spectra were acquired under magic angle conditions<sup>27,28</sup> to determine the  $\text{sp}^2/\text{sp}^3$  ratio of carbon bonds. For every sample 50 spectra were taken at 10 different arbitrary selected positions. HOPG was used as a reference sample with 100%  $\text{sp}^2$  bond.

## Results and Discussion

**Raman Microspectroscopic Analysis of Soot.** The first-order Raman spectra of soot and related carbonaceous materials are characterized by two broad and strongly overlapping peaks with intensity maxima near 1580  $\text{cm}^{-1}$  (G or “graphite” peak) and 1350  $\text{cm}^{-1}$  (D or “defect” peak). The G mode of graphite has  $E_{2g}$  symmetry and involves the in-plane bond-stretching motion of pairs of  $\text{sp}^2$ -hybridized carbon atoms.<sup>17</sup> The D peak is associated with the breathing mode of  $A_{1g}$  symmetry. It is known to be characteristic for disordered graphite, and its intensity increases relative to the G peak with increasing degree of disorder in the graphitic structure.<sup>13,29</sup>

Figure 1 shows the Raman spectra of untreated (298 K) and oxidized (773 K) samples. Each spectrum corresponds to the average of seven spectra; thus it is highly representative for each sample. For a better comparison of the two broad overlapping G and D peaks, the spectra were normalized to the intensity of the G peak. This is possible as due to literature and our own observations, no significant dispersion was found for G mode of soot and at crystalline graphite. In contrast to the G peak, whose position stays constant with respect to  $\lambda_0$ , the D peak shifts to lower energy and its relative intensity (compared to G peak) increases as  $\lambda_0$  changes from 514 to 633 nm as will be illustrated later. The peaks in the spectra of graphite are completely separated and show a large G peak around 1580  $\text{cm}^{-1}$  and a small D peak around 1350  $\text{cm}^{-1}$ . The spectra of GfG, EURO VI, and EURO IV soot ( $\lambda_0 = 514 \text{ nm}$ ) show two broad and overlapping peaks around 1580 (G peak) and 1350  $\text{cm}^{-1}$  (D peak) that are typical for soot and related carbonaceous materials. Compared to untreated GfG soot, which shows very broad and strongly overlapping peaks, the Raman spectra for EURO VI and EURO IV with more separated G and D peaks

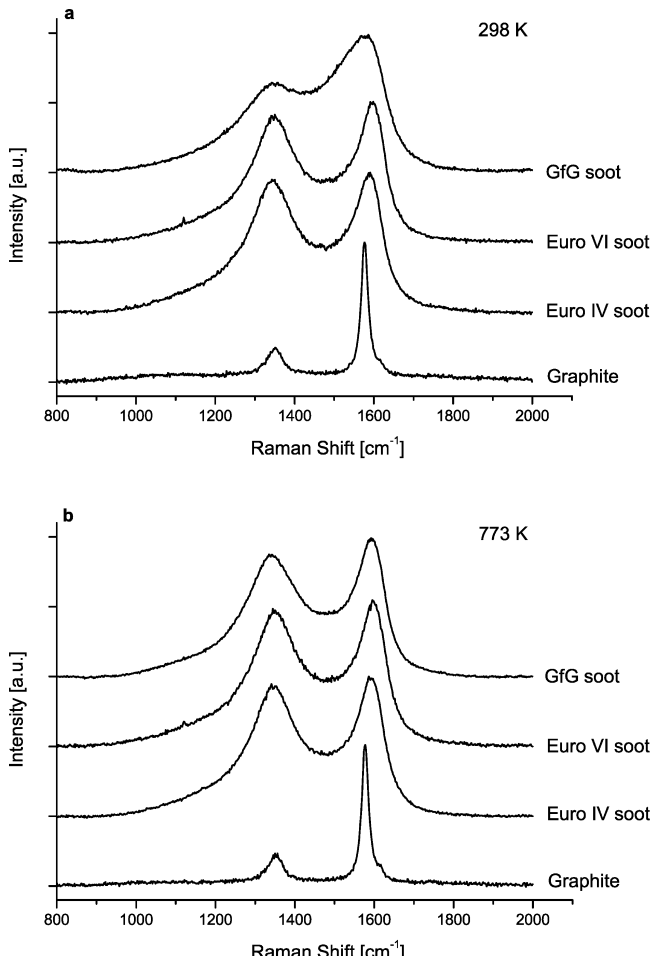


**Figure 1.** Raman spectra ( $\lambda_0 = 514 \text{ nm}$ ) of untreated (a) and oxidized (b) GfG soot, EURO VI soot, EURO IV soot, and graphite powder.

imply a more homogeneous structure with a lower content of molecular carbon.

For GfG soot the peaks became narrowed during oxidation, whereas the spectra of EURO VI and EURO IV soot remained largely unchanged (Figure 1). As expected no changes were found in spectra of graphite after oxidation up to 773 K. The different behavior of GfG soot on one hand and EURO VI and EURO IV soot on the other hand can be explained by differences in their structure. This assumption is in good agreement with HRTEM analysis of untreated and oxidized GfG, EURO VI, and EURO IV soot as discussed later. Moreover, it was already shown that untreated GfG soot possesses a more heterogeneous and functionalized structure than EURO IV soot. In GfG soot the high amount of defects and deviation of the carbons from a perfect graphitic structure results in an increased surface functionalization.<sup>9</sup>

**Changes of Spectral Parameters upon Oxidation.** For quantitative spectral analysis the five band fitting procedure proposed by Sadezky et al.<sup>13</sup> was applied. Band position (Stokes shift,  $\text{cm}^{-1}$ ), full width at half-maximum (fwhm,  $\text{cm}^{-1}$ ), and integrated band intensity relative to the G band ( $I/I_G$ ) were determined from the spectra of untreated and oxidized soot samples. An exemplary spectrum of untreated EURO IV soot with five band fits is shown in Figure 2. Overall, the spectral parameters obtained for untreated graphite and GfG soot are in agreement with those reported by Sadezky et al.<sup>13</sup>

The D1 band has been suggested to arise from carbon atoms of a graphene layer in immediate vicinity of a lattice disturbance.

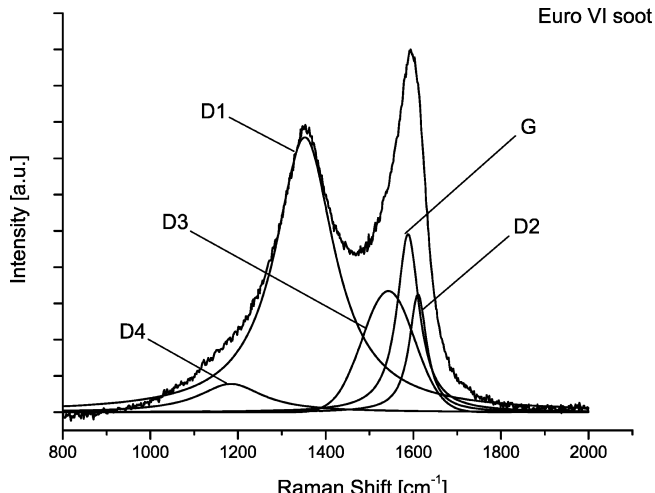


**Figure 2.** Exemplary spectrum ( $\lambda_0 = 514 \text{ nm}$ ) of untreated EURO VI soot with five band fits.

The D3 band has been associated with the molecular carbon content of soot. It has been shown that D1 fwhm and D3 band intensity are the spectroscopic parameters which can provide information about the relative abundance and structural order of graphite-like and molecular carbon and give most information about the chemical structure<sup>18</sup> and reactivity of different types of soot.<sup>19,26</sup> Moreover it has been found that the D1 bandwidth exhibits a nearly linear negative correlation with the amount of apparent elemental carbon in different types of soot and related carbonaceous materials.<sup>18</sup> Therefore in the present study we focused predominantly on discussions of changes in the D1 fwhm and the D3 band relative intensity during oxidation.

For GfG soot (Figure 1) the relative intensity of the D3 band around  $1500 \text{ cm}^{-1}$ , which is responsible for the strong overlap of G and D peaks, is decreasing and the two observed Raman peaks are getting more separated during the TPO. Also the intensity of D peak (the sum of D1 and D4 bands), is increasing with higher temperature, while the position stays constant. On the other hand the G peak (the sum of G and D2 bands) shows a blue shift after the oxidation. D1, G and D2 are narrowing their fwhm, indicating an increase of structural order and a decrease of chemical heterogeneity of GfG soot upon oxidation. Untreated EURO VI and EURO IV soot present spectra that are quite different in comparison to GfG soot. The two Raman peaks are more separated, and the band's fwhm is generally smaller. After oxidation up to 773 K the relative intensity and the fwhm of the overall G and D peak of EURO VI and EURO IV are not significantly changed.

Figure 3a shows fwhm of the D1 band (associated with disordered graphitic lattice vibrations) for untreated and oxidized GfG soot, EURO VI soot, EURO IV soot, and graphite. For untreated GfG soot the fwhm of D1 band lies at around  $225 \pm 7 \text{ cm}^{-1}$  and remains in the range of the standard deviations until about 673 K. Then it decreases down to  $170 \pm 6 \text{ cm}^{-1}$  at 773 K. This progressive decrease of D1 fwhm indicates a decrease of chemical heterogeneity and an increase of structural order as reported previously for comparable studies.<sup>18,26</sup> The lower starting values for EURO VI soot at  $158 \pm 5 \text{ cm}^{-1}$  and EURO IV soot at  $145 \pm 3 \text{ cm}^{-1}$  indicate a much lower degree of chemical heterogeneity and structural disorder compared to GfG soot ( $225 \pm 7 \text{ cm}^{-1}$ ). A slight decrease of D1 fwhm upon oxidation can be observed for EURO VI soot, whereas the changes in D1 fwhm of EURO IV soot stay within standard deviation values. The final value at 773 K lies at  $145 \pm 3 \text{ cm}^{-1}$ .

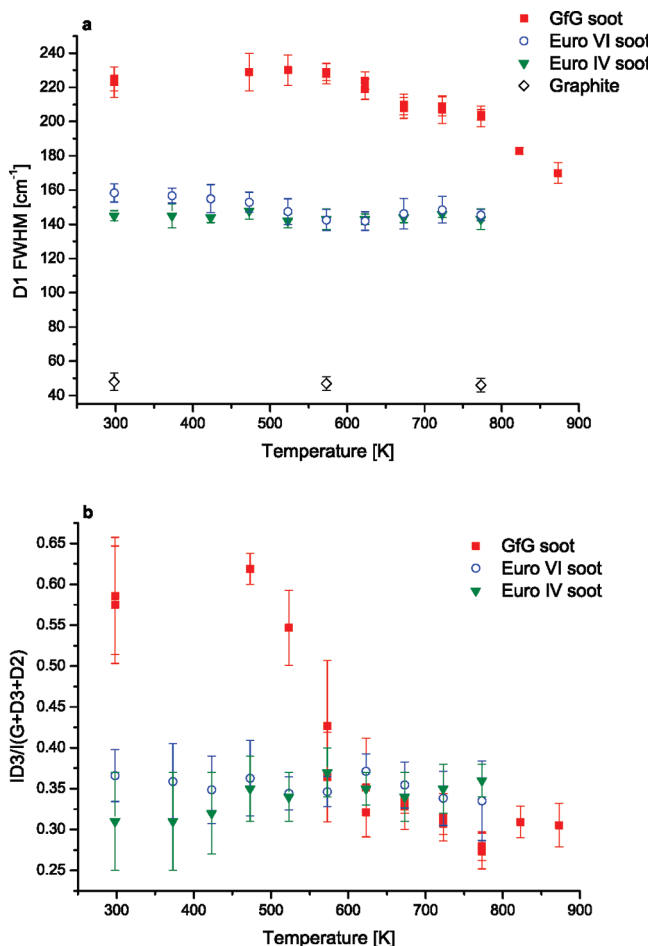


**Figure 3.** Changes in fwhm of D1 band (a) and relative intensity of D3 band (R3) (b) for GfG soot, EURO VI soot, EURO IV soot, and graphite powder during oxidation versus temperature.

for EURO VI soot and at  $143 \pm 5$  cm<sup>-1</sup> for EURO IV soot. The higher initial value of D1 fwhm and the slight changes upon oxidation for EURO VI soot compared to EURO IV soot suggest a more disordered and hence slightly more reactive structure for EURO VI soot. The values for D1 fwhm for graphite around  $47 \pm 4$  cm<sup>-1</sup> are much lower compared to all soot samples analyzed in this study. As expected, graphite seems to show the highest degree of structural order and should be characterized by lower reactivity.

The relative intensity of the D3 band ( $R3 = I_{D3}/(I_{D3} + I_{D2} + I_G)$ )<sup>19,26</sup> has been calculated and plotted against temperature as shown in Figure 3b. A rapid decrease of the D3 band relative intensity for GfG soot from  $0.57 \pm 0.07$  at 293 K to  $0.33 \pm 0.05$  at 623 K indicates a decrease of molecular carbon content. From 623 K the R3 value remains constant in the range of standard deviations. For EURO VI and EURO IV soot the starting values of the R3 parameter ( $0.36 \pm 0.03$  for EURO VI and  $0.32 \pm 0.07$  for EURO IV) are much lower than the value for GfG soot. That indicates a lower content of molecular carbon in EURO VI and EURO IV soot. During the oxidation, the changes in the mean values of the D3 band relative intensity hardly exceeded the standard deviations. The variations for R3 parameter can be associated with structural differences between various measurement points. For graphite the R3 parameter was not determined, because no peak overlap and thereby no D3 band can be found in the spectra, since graphite is free of molecular carbon.

### Structural Analysis Based on the Dispersive Character of D Mode.

First-order Raman spectra (800–2000 cm<sup>-1</sup>) of highly ordered pyrolytic graphite (HOPG) obtained by laser excitation wavelengths ( $\lambda_0$ ) 514 and 633 nm are shown in Figure SI1 (see Supporting Information). Similar spectra exhibit only one G peak at 1579 cm<sup>-1</sup> corresponding to an ideal graphitic lattice vibration. This mode does not require the presence of 6-fold rings and therefore it occurs at all sp<sup>2</sup> sites, not only at those in rings.

Figure SI2 (see Supporting Information) illustrates the spectra of untreated (298 K) and oxidized (773 K) graphite powder. Besides the strong G mode, an additional first-order D peak can be observed around 1350 cm<sup>-1</sup>. The D peak is associated with the breathing mode of A<sub>1g</sub> symmetry, involving phonons near the K zone boundary.<sup>17</sup> This mode is forbidden in perfect graphite (HOPG) and only becomes active in the presence of disordered structures. In contrast to the G mode, the D peak is dispersive (Figure SI2 in Supporting Information). In spectra of untreated and oxidized graphite powder its position shows a similar red shift (from ca. 1350 to 1330 cm<sup>-1</sup>) with increasing of  $\lambda_0$  from 514 to 633 nm.

The dispersive character of the D mode (the shift with excitation energy at a rate of 40–50 cm<sup>-1</sup>/eV over a wide  $\lambda_0$  range) is well-known and was found in different kinds of carbon materials, such as crystalline graphite, glassy carbon, annealed hydrogenated amorphous carbon, multicomponent carbon films, and carbon nanotubes.<sup>30–40</sup> Wang et al. have assumed that the laser wavelength dependence of D band frequency results from scattering from different populations of phonons (subpopulations of phonons scatter different incident photons with different wavelength).<sup>31</sup> Moreover the authors have found that the intensity of the D band relative to the G band varies with carbon type, but the position of the D band at distinct  $\lambda_0$  does not vary for different carbons (graphite and glassy carbon). An approach to explain this excitation-energy dependence of the D mode proposed by Castiglioni et al. is based on the lattice dynamics of small aromatic molecules and their Raman spectra.<sup>40</sup> In these molecules, which can be viewed as small graphitic flakes, the D mode has a Raman-active eigenvector. Its frequency depends on the actual size and shape of the molecule in question. The shift depending on the excitation energy results from a resonant selection of a particular molecule by the incoming laser light. Matthews et al. have explained the origin and dispersion of the D mode in terms of the resonant Raman coupling between electrons and phonons with the same wave vector near the K point of the Brillouin zone.<sup>32</sup> The high dispersion has been ascribed to the coupling between the optical phonons associated with the D peak and the transverse acoustic branch. Reich and Thomsen have attributed the dispersive character of the D mode to the double-resonant Raman process, which for a given laser energy and phonon branch selectively enhances a particular phonon wave vector and phonon frequency.<sup>34</sup> The authors have underlined that the double-resonance condition depends strongly on the wave vector of the photoexcited electrons and holes and hence on excitation energy. To address the problem of the dispersion of D peak, Sood et al. have proposed disorder-induced two-phonon scattering (combination of an optic photon at the K point in the Brillouin zone and acoustic phonon whose momentum is determined uniquely by the double resonance condition) and the double resonance.<sup>35</sup>

It should be mentioned that for different graphite and soot samples the D mode is dispersive, while the position of the G peak is invariant.<sup>13,17,30–32,36,37</sup> It was already pointed out that for soot the heterogeneous structure of samples has to be taken

into account. In this case only the graphitic (but not molecular) part should have impact on the dispersive character of the D peak. The detailed structural analysis of soot samples by HRTEM and EELS can help to understand the origin of the D mode in Raman spectra. The dispersive D peak may be a superposition of molecule and graphitic contribution.

On the other hand, dispersion of the G mode occurs in the case of amorphous (a-C), hydrogenated a-C, and tetrahedral amorphous carbon (ta-C) samples. In the spectra of the a-C the G peak moves to ca.  $1610\text{ cm}^{-1}$  ( $\lambda_0 = 514\text{ nm}$ ) and the relative intensity of the D peak becomes very low ( $I_D/I_G \rightarrow 0$ ) compared with soot and graphitic samples. For the ta-C the G peak is located at ca.  $1570\text{ cm}^{-1}$  (or  $1630\text{ cm}^{-1}$ ) and  $I_D/I_G$  is very low or zero.<sup>17,36,41</sup>

Figures SI3–SI5 (see Supporting Information) show the Raman spectra of EURO IV and VI diesel soot as well as GfG spark discharge soot before (at 298 K) and after oxidation (up to 773 K) measured at 514 and 633 nm. A similar dispersive behavior of the D mode was found for untreated EURO IV and VI soot compared to oxidized samples, suggesting no noticeable structural changes upon oxidation (Figures SI3 and SI4 in Supporting Information). For untreated GfG soot (Figure SI5a in Supporting Information) relative intensity of the D peak increases obviously stronger than for EURO IV and VI soot with increasing  $\lambda_0$ , indicating differences in the structure of untreated spark discharge and diesel soot samples. Moreover, we found that significant spectral differences measured at 514 and 633 nm for untreated soot are not that evident for the oxidized sample (Figure SI5b in Supporting Information). The D peak becomes narrower, whereas its relative intensity shows a smaller difference in spectra collected with Ar<sup>+</sup> and He–Ne laser. The significant changes in GfG soot spectra after oxidation can be explained by changes in soot structure due to a preferential oxidation of molecular carbon that led to an increase of chemical homogeneity and graphitic order.

In order to compare the behavior of the D mode for untreated and oxidized graphite powder, EURO IV and VI, and GfG soot, the differences of spectra measured at 514 and 633 nm are plotted in Figure 4. As expected, the lowest differences are found for untreated graphite powder (Figure 4a). For difference spectra of EURO IV and VI, the similar intensive and broad (from ca. 1000 to  $1400\text{ cm}^{-1}$ ) signatures are characteristic. The untreated GfG soot shows largest differences in spectra (from ca. 1000 to  $1500\text{ cm}^{-1}$ ) obtained with Ar<sup>+</sup> and He–Ne lasers. Obviously, the grown differences in spectra of graphite, EURO IV and VI, and GfG soot measured at 514 and 633 nm can be explained by an increasing degree of disorder and/or molecular content from graphite powder to GfG soot. No significant changes can be found in difference spectra of graphite powder and EURO IV and VI soot samples before and after oxidation (Figure 4). Oxidized GfG soot reveals a lower intensity in difference spectrum, compared to untreated GfG soot and EURO IV and VI soot samples, indicating a significant increase in structural order of GfG soot during oxidation.

Table SI1 (see Supporting Information) summarizes the fwhm of G and D1 and relative intensity of D3 as well as G, D1, and D3 band positions obtained by the five band fitting procedure. The position and fwhm of the G band stay invariant in the range of standard deviations (at ca.  $1580\text{ cm}^{-1}$ ) for all analyzed samples as  $\lambda_0$  has been changed from 514 to 633 nm. The relative intensity of D3 shows also no significant variations due to change of  $\lambda_0$  for EURO IV and VI soot samples. The D1 band (that mostly coincides with observed D peak) exhibits obvious dispersive character. The position of this band shows

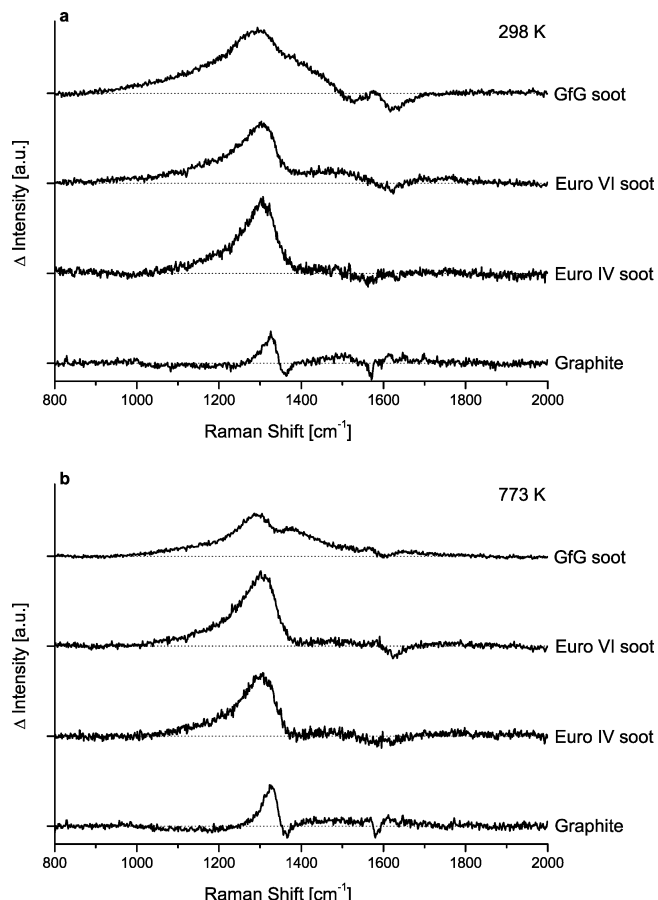


**Figure 4.** Difference spectra obtained at  $\lambda_0$  514 and 633 nm for untreated (a) and oxidized (b) graphite powder, EURO IV and VI, and GfG soot (range  $1000$ – $1500\text{ cm}^{-1}$ ).

a ca.  $20\text{ cm}^{-1}$  red shift (from ca.  $1350$  to ca.  $1330\text{ cm}^{-1}$ ) for spectra of graphite powder and EURO IV and VI soot samples before and after oxidation measured at 514–633 nm. For untreated GfG soot, ca.  $30\text{ cm}^{-1}$  red shift is observed (from  $1346 \pm 3$  to  $1317 \pm 3\text{ cm}^{-1}$ ), whereas for oxidized sample the shift decreases down to  $20\text{ cm}^{-1}$  (from  $1355 \pm 1$  to  $1335 \pm 1\text{ cm}^{-1}$ ). The differences between relative intensity of D3 band in spectra of untreated GfG soot obtained with Ar<sup>+</sup> and He–Ne laser also become extinct for oxidized soot. The obvious changes in dispersion for spectra of GfG soot before and after oxidation suggest pronounced differences in the structure of those samples. Thus, we can conclude that the dispersive character of the D mode can be applied for structural analysis of soot and related carbonaceous materials.

**HRTEM Analysis of Soot upon Oxidation.** TEM and HRTEM investigations were carried out to deduce the microstructure of the different soots. We focused on comparable structural analysis of untreated and oxidized graphite powder and EURO IV, EURO VI, and GfG soot samples. It should be mentioned that our HRTEM data for untreated GfG and EURO IV soots are in good agreement with recent studies reported by Su et al.<sup>10</sup> and Müller et al.<sup>8,42</sup>

HRTEM reveals that the samples contain, besides graphene BSUs, twisted ribbons with molecular units “sitting” on them. As the investigated particles are thicker than the depth of focus in the microscope, the two-dimensional projection may lead to less straightforward interpretation. The projection of the three-dimensional objects may indicate that some graphitic structure is present, which is in the case of GfG, Euro VI, and Euro IV only due to the selected defocus value. In particular the contrast

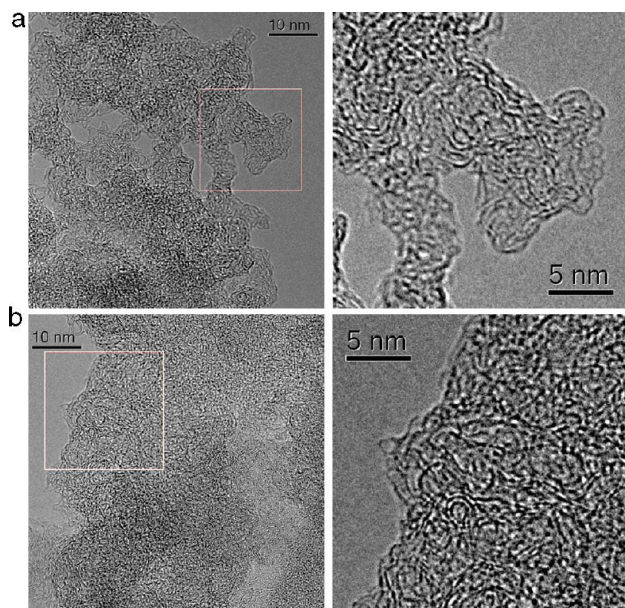


**Figure 5.** Overview and enlarged HRTEM images of untreated (a) and oxidized (b) GfG soot.

“gaps” following the rounded contour of a “graphene” layer arises from tilting of the graphene ribbon with respect to the projection. Multiple segmentation seems to indicate apparent small BSU. For a detailed description see ref 43.

High-resolution micrographs of the untreated GfG soot (Figure 5a) show very fine agglomerates. The graphene segments are strongly bent and connected to long chainlike agglomerates, which is in good agreement with previous studies.<sup>8,42</sup> Observations on the untreated GfG soot the micrographs of the sample oxidized up to 773 K (Figure 5b) show less chainlike orientation. The particles seem “tighter” connected than the untreated one, suggesting an increase of structural order for GfG soot upon oxidation.

Micrographs of the untreated and oxidized EURO VI sample reveal a more pronounced long-range order and higher structural order compared to untreated GfG soot. On the surface of the untreated EURO VI soot (Figure 6a) small fullerenoid particles with an onion-like structure can be observed. These particles are similar to those found on the EURO IV sample as discussed later. After the oxidation process the EURO VI sample (Figure 6b) does not show significant modifications. In this case the oxidation and heat treatment seem to have no direct observable effect on the microstructure of the soot particles.

No distinct morphological differences were found between EURO IV and EURO VI soot. There is a similar arrangement of graphene layers explained by a similar soot formation process characterized by oxygen-lean high-temperature conditions. In both untreated and oxidized EURO IV samples, small fullerenoid-like particles with a diameter of 1–3 nm were found at the surface. Similar structures were recently reported for untreated EURO IV soot.<sup>8,10,42</sup> On the surface of as-collected soot particles, poorly ordered carbon is present (Figure 7a), which is preferentially removed during the oxidizing and heating process up to 773 K (Figure 12b). The preferential oxidation of the highly disordered fraction should lead to an apparent increase in overall ordering if its volume fraction was significant in the deep parts of the secondary structure. This suggests that the heat treatment and oxidation result in the removal of these minor present molecular layers, which should slightly modify the overall order and graphitization of the EURO IV soot. HRTEM of the graphite

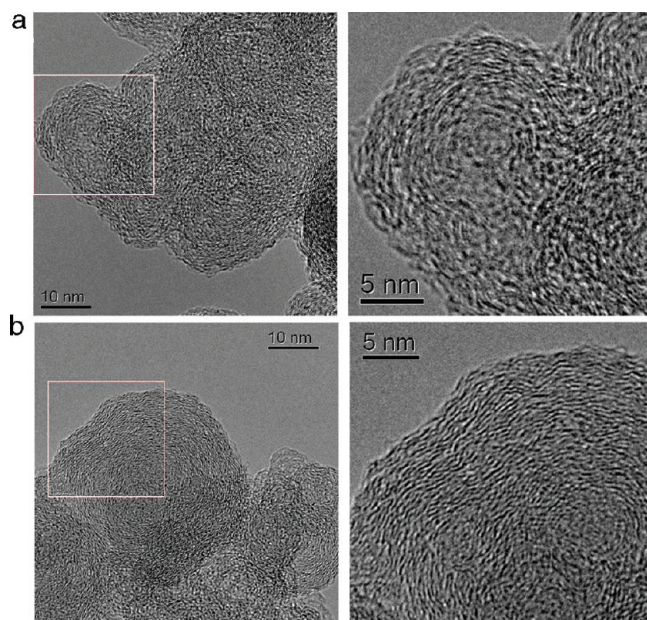


**Figure 6.** Overview and enlarged HRTEM images of untreated (a) and oxidized (b) EURO VI soot.

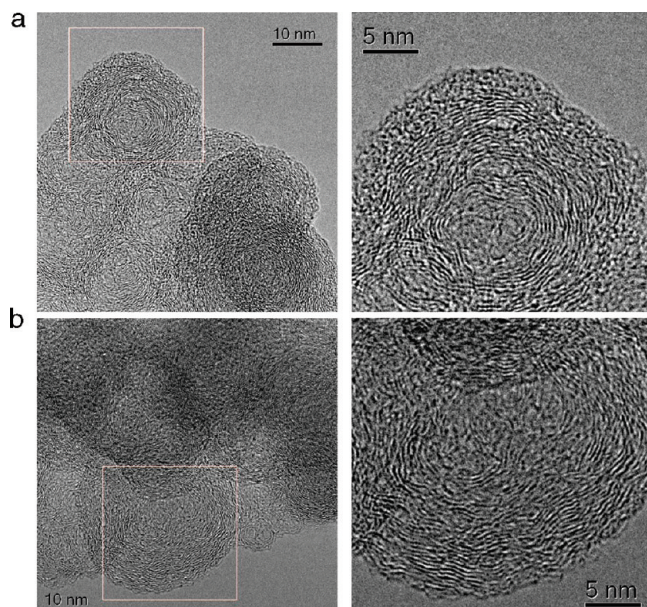


**Figure 7.** Overview and enlarged HRTEM images of untreated (a) and oxidized (b) EURO IV soot.

powder sample (Figure 8) shows only minor morphological differences before and after oxidation. The sample is composed of stacks of graphene layers with some molecular-type carbon on the surface of the untreated sample. This sample exhibits over the predominant volume well-defined long-range ordering, being in contrast to the GfG, EURO IV, and EURO VI samples. Due to its graphitic structure, the sample is expected to be much less reactive than the other samples.

Particle sizes were counted for diesel soot samples (EURO VI and IV) to determine how the thermal and oxidation treatment affects the distribution of secondary structural parameters. Due to the fact that the secondary soot particles cluster together to build agglomerates with sizes outside the depth of resolution of the HRTEM, it was necessary to confine counting to the outer parts of the agglomerates where it is still possible to determine the individual sizes of the particles. The quantitative

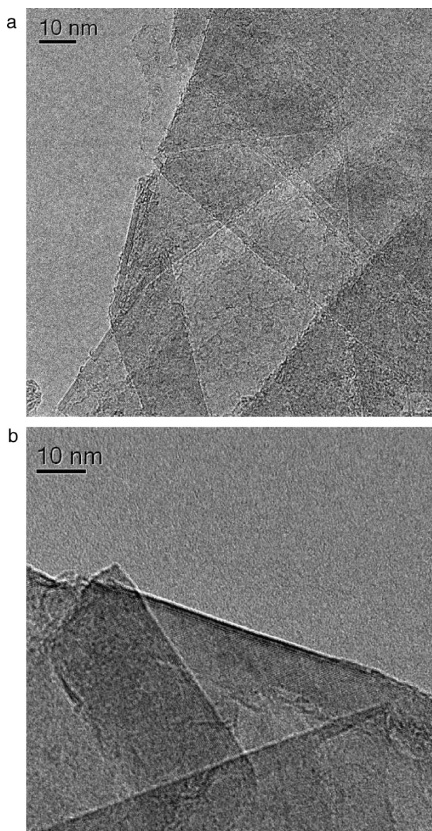


**Figure 8.** HRTEM images of untreated (a) and oxidized (b) graphite powder.

**TABLE 1: Mean Values and Standard Deviations of Curvature and Radii Distribution of the Soot Particles**

	curvature (nm)		radius (nm) <sup>a</sup>	
	MV	SD	MV	SD
GfG untreated	0.607	0.117	n. a.	n. a.
GfG oxidized	0.627	0.119	n. a.	n. a.
Euro VI untreated	0.650	0.107	12	4
Euro VI oxidized	0.666	0.106	12	3
Euro IV untreated	0.674	0.076	14	6
Euro IV oxidized	0.709	0.082	11	3

<sup>a</sup> n. a., not analyzed.

morphological characterizations of EURO IV and EURO VI are summarized in Table 1. The mean radii of Euro IV and VI soot are calculated from the mean size of the particles. The obtained mean radii for the untreated EURO VI and IV soot samples are  $12 \pm 4$  and  $14 \pm 6$  nm, respectively. After the heat and oxidation treatment, the radii of the EURO IV particles only slightly decrease ( $11 \pm 3$  nm) and stay constant for the EURO VI particles ( $12 \pm 3$  nm). Within the given error bars, it can be mentioned that the size of the soot particles remains almost unchanged.

Consequently the oxidation occurs in a transport-limited way and progresses with a reaction front from the outer surface of the tertiary structure (agglomerate). The secondary structure is oxidized sphere by sphere and no extensive concerted oxidation throughout the bulk of the sample occurs. This precludes the abundance of highly reactive poorly ordered or molecular carbon as a binder place between the supramolecular twisted graphene ribbons. A reactive binder place would have led to porosity and thus to simultaneous shrinkage of all remaining secondary structural units.

The curvature of graphene ribbons is an important indicator for its defect content creating deviations from planarity and hence affecting its reactivity. This was shown earlier for other materials<sup>42</sup> where also details of the measuring procedure are described. It is important to point out that only the fraction parallel to the electron beam projecting ribbon elements and not “graphene units” weakly interconnected as intuitively assumed from observing the HRTEM images are evaluated. Curvature is defined as the length ratio between an uninterrupted contrast line of a ribbon and the shortest distance between its terminal points.

The results of the statistical measurements of the curvature analysis for GfG, Euro VI, and Euro IV soots are listed in Table 1. A clear trend can be seen for the different samples. The untreated GfG sample is by far the sample which is bent strongest. After the heat and oxidation treatment, the curvature flattens allowing the conclusion of a better ordering and reduced reactivity; the material is expected to self-inhibit its oxidation. This is in good agreement with results obtained by TPO. The EURO VI and IV samples show higher values for the curvature index indicating weaker bending as compared to the untreated GfG soot. During the oxidation treatment the curvature for EURO VI and IV soots weakly decreases within in the range of its standard deviations. A slightly higher bending for untreated and oxidized EURO VI soot compared to EURO IV soot suggests that EURO VI soot can be characterized by higher defect density and thus by some higher functionalization.<sup>42</sup> This is in good agreement with TPO and Raman data.

**EELS of Soot upon Oxidation.** EELS was applied to reveal information about the average electronic structure of the sample. To determine the hybridization of the carbon bonds and their changes upon oxidation, the spectra were taken under magic angle conditions.<sup>42</sup> The EEL spectrum of HOPG was acquired as a standard for sp<sup>2</sup>-bonded carbon. The spectra of the analyzed samples were then fitted with three Gauss curves<sup>42</sup> to determine the area under the curves used for quantifying the ratio of sp<sup>2</sup> to sp<sup>3</sup> bonds in the soot samples (see Figure SI6 and Table SI2 in Supporting Information). Figure 9 displays the EEL spectra of the investigated samples acquired under magic angle conditions. The features visible in the carbon K-edge represent different components of unoccupied electronic states. The  $\pi^*$  feature at an energy loss of  $\sim 285$  eV represents transitions of C 1s electrons to unoccupied  $\pi^*$  whereas the  $\sigma^*$  feature at  $\sim 291$  eV reflects that of transition to unoccupied  $\sigma^*$  state. The  $\pi^*$  feature is typical for an sp<sup>2</sup>-hybridized carbon. The percentage of sp<sup>2</sup>-bonded carbon of these samples calculated according to eq 1 is displayed in Figure 10.

$$\text{sp}^2 = \frac{\left[ \frac{\text{area}(\pi^*)}{\text{area}(\pi^* + \sigma^*)} \right]_{\text{sample}}}{\left[ \frac{\text{area}(\pi^*)}{\text{area}(\pi^* + \sigma^*)} \right]_{100\% \text{sp}^2 \text{reference}}} \quad (1)$$

The results for untreated GfG soot indicate a good correlation between HRTEM and EELS data. The poor parallel alignment of the graphene units visible in Figure 5a fits quite well to the low abundance of sp<sup>2</sup>-bonded carbon in the sample as obtained by EELS. GfG soot undergoes a change in its microstructure during the oxidation process, which leads to a substantial increase of the degree of graphitization. The abundance of sp<sup>2</sup>-bonded carbon increases from an initial value at room temperature of 56% to a final value of 79% in the treated sample. EURO VI shows nearly no changes in hybridization before (89%) and after heat treatment (88%), which is in good agreement with

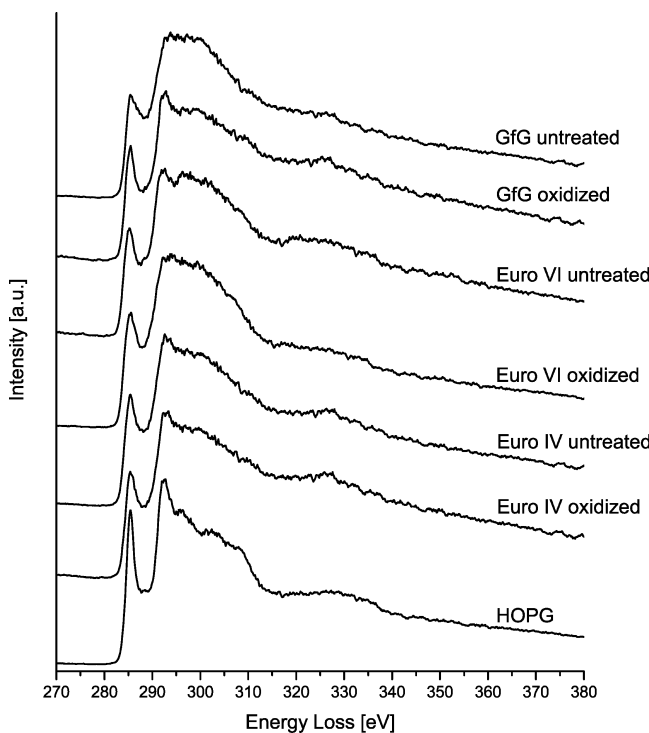


**Figure 9.** EEL spectra taken under magic angle conditions for GfG soot, EURO VI soot, EURO IV soot, and HOPG.

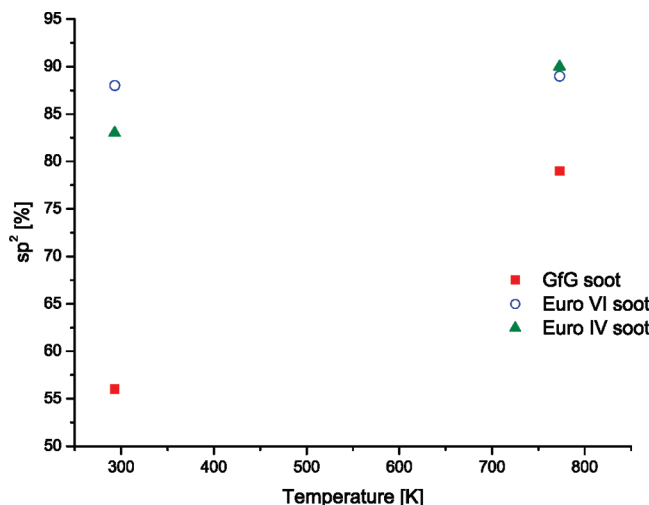


**Figure 10.** Changes of the sp<sup>2</sup> ratio for GfG soot, EURO VI soot, and EURO IV soot with increasing temperature.

RM data. The higher initial amount of sp<sup>2</sup>-bonded carbon in the EURO VI sample compared to that in the EURO IV sample is seen in the slightly more pronounced  $\pi^*$  presence at 285 eV. Relative to that, the EURO IV sample shows an increase in graphitization degree upon oxidation treatment from 83% to 90% sp<sup>2</sup> bond. This is in agreement with the HRTEM investigation that explains this increase in graphitization of EURO IV by the removal of minor present molecular layers and by slight changes in the curvature of the sample. The flattening of the graphene layers during the heat treatment fits with the increase of the fraction of sp<sup>2</sup>-hybridized carbon atoms in the sample.

**Mass Conversion of Soot upon Oxidation.** During the TPO, FTIR spectra were constantly taken to get an overview about the CO<sub>2</sub> emission and thereby the reactivity of the oxidized soot. Figure 11 shows the mass conversion over time, which has been calculated by the CO<sub>2</sub> evolution from GfG, EURO VI, EURO IV, and graphite during TPO up to 773 K with a heating rate

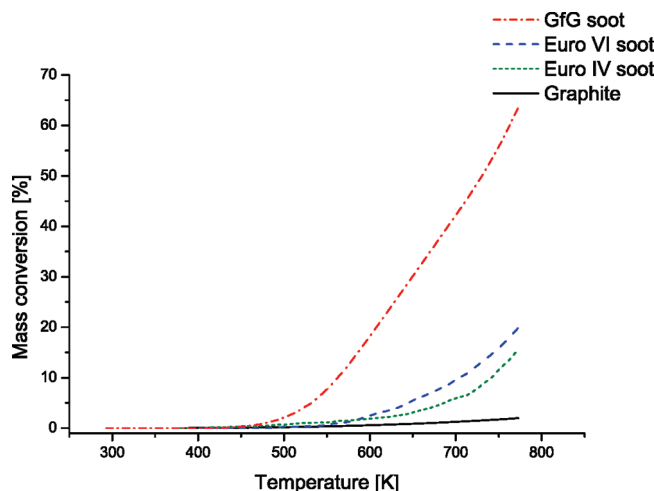


**Figure 11.** Mass conversion ( $1 - m/m_0$ ) versus temperature by oxidation of GfG soot, EURO VI soot, EURO IV soot, and graphite powder up to 773 K, heating rate 5 K/min.

of 5 K/min. The comparison of these curves all arising from significant nominally “pure” carbon reveals differences in their reactivity, which will be associated with differences in structure. GfG soot was found to be the most reactive. Starting from 423 K a low mass loss due to desorption of volatile surface functional groups is observed. A rapid oxidation step, indicating the oxidation of highly reactive strongly curved fullerenoidic and molecular carbon structures starts at about 450 K, showing a mass conversion of ca. 65% at 773 K. The lowest reactivity was observed for graphite, which shows a mass conversion of only 2% at 773 K and is in the range of accuracy of the experiment.

Diesel soot samples exhibited a moderate reactivity. For EURO VI and EURO IV soot the combustion starts at higher temperatures (about 550 K) and seems to proceed much slower compared to GfG soot. At high temperatures (773 K) the amount of soot that is oxidized is much lower in EURO VI (ca. 20%) and EURO IV soots (ca. 15%) than in GfG soot (ca. 65%), suggesting a less reactive structure of EURO VI and EURO IV soots. However, we found a slight increase in reactivity for EURO VI soot compared to EURO IV soot that is in agreement with RM and quantitative HRTEM analysis.

**Reactivity–Structure Correlations of Soot.** In order to analyze the correlations between Raman spectroscopic parameters and soot reactivity, the D1 bandwidth of GfG soot, EURO VI soot, EURO IV soot, and graphite has been plotted against mass conversion ( $1 - m/m_0$ ) determined by gravimetry (Figure 12a). For GfG soot it was found that up to ca. 20% of mass conversion the changes in the mean values of D1 fwhm ( $225 \pm 7 \text{ cm}^{-1}$  for untreated soot) stay in the range of standard deviations. After that, D1 bandwidth decreases slowly (down to  $203 \pm 6 \text{ cm}^{-1}$ ) until 65% of mass conversion corresponding to 773 K, indicating an increase of chemical homogeneity and structural order in the GfG soot sample upon TPO. For EURO VI and EURO IV soot the overall values for D1 fwhm are much lower compared to GfG soot. Only slight or no significant changes upon oxidation were detected for EURO VI and EURO IV soot samples, respectively. The final values for EURO VI soot are around  $145 \pm 3 \text{ cm}^{-1}$  at 20% of mass conversion, which corresponds to 773 K. In the case of EURO IV soot the D1 fwhm lies at  $143 \pm 5 \text{ cm}^{-1}$  at 15% of mass conversion, indicating some lower degree of chemical heterogeneity and structural disorder compared to EURO VI soot. Graphite shows

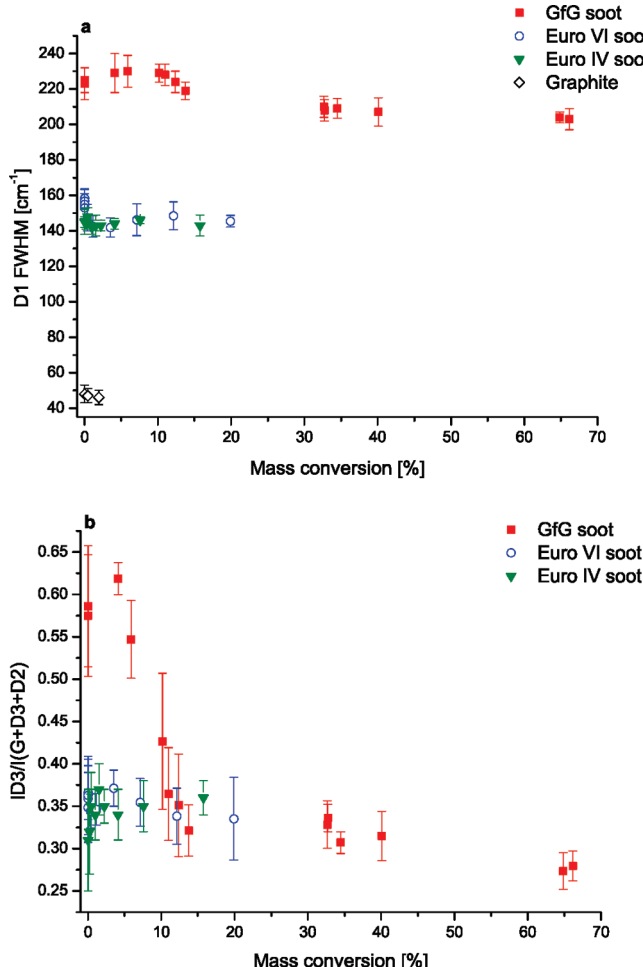


**Figure 12.** Changes in fwhm of D1 band (a) and relative intensity of D3 band (R3) (b) for GfG soot, EURO VI soot, EURO IV soot, and graphite powder during oxidation versus mass conversion.

only 2% of mass conversion and no changes in D1 fwhm after the oxidation process at all.

Figure 12b shows a steep decrease of R3 parameter of GfG soot from  $0.57 \pm 0.07$  at the beginning of the oxidation to  $0.32 \pm 0.03$  at 13% of mass conversion. From about 20% of mass conversion the R3 parameter remains constant until the end of the TPO. This steep decrease suggests preferential oxidation of the highly reactive molecular carbon fraction. The amount of molecular carbon in GfG can be estimated as 20%. For EURO VI and EURO IV soot the overall values for the R3 parameter show no significant changes upon oxidation. The starting values of R3 parameter ( $0.36 \pm 0.03$  for EURO VI and  $0.32 \pm 0.07$  for EURO IV) are much lower than the starting value for GfG soot ( $0.57 \pm 0.07$ ) and stay constant in the range of standard deviations until 20% of mass conversion for EURO VI soot and 15% of mass conversion for EURO IV soot, both corresponding to 773 K. The amount of molecular carbon in EURO VI and EURO IV soot seems to be lower than that for GfG soot.

In conclusion the D3 band relative intensity and D1 bandwidth are well correlated with molecular carbon content and with the structural order in GfG soot. Actually, these two parameters are significantly changing in two different temperature regions. EURO VI and EURO IV soots seem to be partially characterized by well-distinguishable structures like molecular carbon and graphitic lattices. Here the structures seem to be more homogeneous and more organized.

## Implications and Outlook

Information about soot structure and reactivity becomes more important with the development of modern diesel engines that can create more reactive soot particles. Knowledge about the structure of soot can be used for investigation and optimization of diesel exhaust aftertreatment systems. Moreover, this information can help to understand the influence of soot particles on environmental chemistry, climate, and public health.

In this study we combined RM, TPO, HRTEM, and EELS to investigate changes in structure and reactivity of soot during oxidation by oxygen at increasing temperatures. We analyzed the correlation between structure and reactivity of GfG, EURO VI, and EURO IV soots and graphite powder with different analytical methods to get an overview on the relationship between structure and reactivity of soot particles in diesel exhaust. On the other hand, detailed structural analysis of the soot samples before and after oxidation by HRTEM and EELS allowed us to get better insight into complex heterogenous structure of soot and to understand the origin of G and D modes in Raman spectra.

We found, that the observed Raman spectra of untreated EURO VI and EURO IV soot samples are quite different in comparison to spectra of GfG soot. The two Raman peaks are more separated, which implies a more homogeneous structure with a lower content of molecular carbon for EURO VI and EURO IV soots than for GfG soot. Also the analysis of Raman spectroscopic parameters show a higher degree of disorder and a higher amount of molecular carbon for untreated GfG soot samples than for untreated EURO VI and EURO IV soots. The higher initial value of D1 fwhm and the slight changes upon oxidation for EURO VI soot compared to EURO IV soot suggest a more disordered and hence slightly more reactive structure for EURO VI soot. This is in good agreement with curvature analysis data based on HRTEM images.

The structural analysis based on the dispersive character of the D mode shows grown differences in spectra of graphite powder and EURO IV, VI, and GfG soots measured at 514 and 633 nm, which can be explained by an increasing degree of disorder and/or molecular content from graphite powder to GfG soot. The obvious changes in dispersion for spectra of GfG soot before and after oxidation suggests changes in the structure of those samples, whereas no significant changes can be found in difference spectra of graphite powder and EURO IV and VI soots samples before and after oxidation.

Additional to that, HRTEM investigations were carried out to deduce the microstructure of the different soot samples. The EURO IV and VI samples show a different morphology compared to GfG soot. Micrographs of the untreated EURO IV and EURO VI soot sample reveal a more pronounced long-range order and higher structural order compared to GfG soot.

The reactivity of the investigated samples can be determined by measuring the curvature of the graphene layers. The GfG sample is by far the sample which is bent strongest. EURO IV and VI samples show higher values for the curvature which indicates that the bending is weaker. A slightly higher bending for untreated and oxidized EURO VI soot compared to EURO IV soot suggests that EURO VI soot can be characterized by some higher functionalization and therefore some higher reactivity. This is in good agreement with TPO data.

The analysis of mass conversion of the samples shows significant differences in their reactivity, which can be associated with differences in structure. GfG soot was found to be the most reactive. EURO IV and VI soot samples exhibited a moderate reactivity. We found a slight increase in reactivity for EURO

VI soot compared to EURO IV soot that is in agreement with RM and HRTEM data (curvature analysis). It has to be mentioned that high reactivity may lead to higher toxicity as shown in literature.<sup>44</sup>

Overall, we have demonstrated that the combination of RM, TPO, and HRTEM is useful to get a better knowledge of the structure-reactivity correlations and can help to establish Raman microspectroscopy as a rapid analytical tool to predict reactivity of soot by analyzing the structure. Especially the dispersive character of the D mode can be applied for structural analysis of soot and related carbonaceous materials.

**Acknowledgment.** Financial support by DFG (NI 261/21-1 and SCHL 332/10-1) is gratefully acknowledged.

**Supporting Information Available:** Additional data associated with analysis of soot structure. This information is available free of charge via the Internet at <http://pubs.acs.org>.

## References and Notes

- (1) Bernstein, J. A.; Alexis, N.; Barnes, C.; Bernstein, I. L.; Bernstein, J. A.; Nel, A.; Peden, D.; Diaz-Sanchez, D.; Tarlo Susan, M.; Williams, P. B. *J. Allergy Clin. Immunol.* **2004**, *114*, 1116.
- (2) Sydbom, A.; Blomberg, A.; Parnia, S.; Stenfors, N.; Sandstrom, T.; Dahlen, S. *Eur. Respir. J.* **2001**, *17*, 733.
- (3) Higgins, K. J.; Jung, H.; Kittelson, D. B.; Roberts, J. T.; Zachariah, M. R. *J. Phys. Chem. A* **2002**, *106*, 96.
- (4) Messerer, A.; Niessner, R.; Pöschl, U. *Carbon* **2006**, *44*, 307.
- (5) Messerer, A.; Rothe, D.; Pöschl, U.; Niessner, R. *Top. Catal.* **2004**, *30/31*, 247.
- (6) Müller, J. O.; Su, D. S.; Jentoft, R. E.; Wild, U.; Schlögl, R. *Environ. Sci. Technol.* **2006**, *40*, 1231.
- (7) Saracco, G.; Badini, C.; Specchia, V. *Chem. Eng. Sci.* **1999**, *54*, 3035.
- (8) Müller, J. O.; Su, D. S.; Jentoft, R. E.; Kröhnert, J.; Jentoft, F. C.; Schlögl, R. *Catal. Today* **2005**, *102–103*, 259.
- (9) Su, D. S.; Jentoft, R. E.; Müller, J. O.; Rothe, D.; Jacob, E.; Simpson, C. D.; Tomovic, Z.; Müllen, K.; Messerer, A.; Pöschl, U.; Niessner, R.; Schlögl, R. *Catal. Today* **2004**, *90*, 127.
- (10) Su, D. S.; Müller, J. O.; Jentoft, R. E.; Rothe, D.; Jacob, E.; Schlögl, R. *Top. Catal.* **2004**, *30/31*, 241.
- (11) Ivleva, N. P.; Niessner, R.; Panne, U. *Anal. Bioanal. Chem.* **2005**, *381*, 261.
- (12) McCreery, R. L. *Raman Spectroscopy for Chemical Analysis*; John Wiley & Sons: New York, 2000; p 15.
- (13) Sadezky, A.; Muckenhuber, H.; Grothe, H.; Niessner, R.; Pöschl, U. *Carbon* **2005**, *43*, 1731.
- (14) Beyssac, O.; Goffe, B.; Petitet, J.-P.; Froigneux, E.; Moreau, M.; Rouzaud, J.-N. *Spectrochim. Acta, Part A* **2003**, *59A*, 2267.
- (15) Dippel, B.; Jander, H.; Heintzenberg, J. *Phys. Chem. Chem. Phys.* **1999**, *1*, 4707.
- (16) Fang, H. L.; Lance, M. J. *Soc. Automot. Eng. [Spec. Publ.] SP-2004, SP-1898*, 89.
- (17) Ferrari, A. C.; Robertson, J. *Phys. Rev. B: Condens. Matter* **2000**, *61*, 14095.
- (18) Ivleva, N. P.; McKeon, U.; Niessner, R.; Pöschl, U. *Aerosol Sci. Technol.* **2007**, *41*, 655.
- (19) Ivleva, N. P.; Messerer, A.; Yang, X.; Niessner, R.; Pöschl, U. *Environ. Sci. Technol.* **2007**, *41*, 3702.
- (20) Jawhari, T.; Roid, A.; Casado, J. *Carbon* **1995**, *33*, 1561.
- (21) Rosen, N.; Novakov, T. *Nature* **1977**, *266*, 708.
- (22) Sze, S. K.; Siddique, N.; Sloan, J. J.; Escribano, R. *Atmos. Environ.* **2001**, *35*, 561.
- (23) Vander Wal, R. L.; Tomasek, A. J.; Street, K.; Hull, D. R.; Thompson, W. K. *Appl. Spectrosc.* **2004**, *58*, 230.
- (24) Al-Qurashi, K.; Boehman, A. L. *Combust. Flame* **2008**, *155*, 675.
- (25) Song, J.; Alam, M.; Boehman, A. L.; Kim, U. *Combust. Flame* **2006**, *146*, 589.
- (26) Knauer, M.; Carrara, M.; Rothe, D.; Niessner, R.; Ivleva, N. P. *Aerosol Sci. Technol.* **2009**, *43*, 1.
- (27) Hebert, C.; Schattschneider, P.; Franco, H.; Jouffrey, B. *Ultramicroscopy* **2006**, *106*, 1139.
- (28) Jouffrey, B.; Schattschneider, P.; Hebert, C. *Ultramicroscopy* **2004**, *102*, 61.
- (29) Tuinstra, F.; König, J. L. *J. Chem. Phys.* **1970**, *53*, 1126.
- (30) Vidano, R. P.; Fischbach, D. B.; Willis, L. J.; Loehr, T. M. *Solid State Commun.* **1981**, *39*, 341.
- (31) Wang, Y.; Alsmeyer, D. C.; McCreery, R. L. *Chem. Mater.* **1990**, *2*, 557.
- (32) Matthews, M. J.; Pimenta, M. A.; Dresselhaus, G.; Dresselhaus, M. S.; Endo, M. *Phys. Rev. B: Condens. Matter* **1999**, *59*, R6585.
- (33) Thomsen, C.; Reich, S. *Phys. Rev. Lett.* **2000**, *85*, 5214.
- (34) Reich, S.; Thomsen, C. *Philos. Trans. R. Soc. London, Ser. A* **2004**, *362*, 2271.
- (35) Sood, A. K.; Gupta, R.; Asher, S. A. *Los Alamos Natl. Lab., Prepr. Arch., Condens. Matter* **2001**, *1*.
- (36) Ramsteiner, M.; Wagner, J. *Appl. Phys. Lett.* **1987**, *51*, 1355.
- (37) Pocsik, I.; Hundhausen, M.; Koos, M.; Ley, L. *J. Non-Cryst. Solids* **1998**, *227–230*, 1083.
- (38) Kastner, J.; Pichler, T.; Kuzmany, H.; Curran, S.; Blau, W.; Weldon, D. N.; Delameliere, M.; Draper, S.; Zandbergen, H. *Chem. Phys. Lett.* **1994**, *221*, 53.
- (39) Rao, A. M.; Richter, E.; Bandow, S.; Chase, B.; Eklund, P. C.; Williams, K. A.; Fang, S.; Subbaswamy, K. R.; Menon, M.; Thess, A.; Smalley, R. E.; Dresselhaus, G.; Dresselhaus, M. S. *Science* **1997**, *275*, 187.
- (40) Castiglioni, C.; Negri, F.; Rigolio, M.; Zerbi, G. *J. Chem. Phys.* **2001**, *115*, 3769.
- (41) Marcus, B.; Fayette, L.; Mermoux, M.; Abello, L.; Luzeau, G. *J. Appl. Phys.* **1994**, *76*, 3463.
- (42) Müller, J. O.; Su, D. S.; Wild, U.; Schlögl, R. *Phys. Chem. Chem. Phys.* **2007**, *9*, 4018.
- (43) Jenkins, G. M.; Kawamura, K.; Ban, L. L. *Proc. R. Soc. London, Ser. A* **1972**, *327*, 501.
- (44) Su, D. S.; Serafino, A.; Müller, J.-O.; Jentoft, R. E.; Schlögl, R.; Fiorito, S. *Environ. Sci. Technol.* **2008**, *42*, 1761.

JP905639D